

Signal Simulation and Experimental Research on Acoustic Emission using LS-DYNA

Zhang Jianchao^{1, 2*}, Hao Rujiang², Wu Zhe¹, Jim Green³ and Li Shaohua²

¹School of Mechanical, Electronic and Control Engineering, Beijing Jiaotong University, Haidian District, Beijing 100044, China

²Engineering Training Center, Shijiazhuang Tiedao University, 17 Northeast, Second Inner Ring, Shijiazhuang 050043, China

³Department of Electrical and Computer Engineering, University of Miami, Coral Gables FL 33146, United States

Received 11 June 2015; Accepted 21 September 2015

Abstract

To calculate sound wave velocity, we performed the Hsu-Nielsen lead break experiment using the ANSYS/LS-DYNA finite element software. First, we identified the key problems in the finite element analysis, such as selecting the exciting force, dividing the grid density, and setting the calculation steps. Second, we established the finite element model of the sound wave transmission in a plate under the lead break simulation. Results revealed not only the transmission characteristics of the sound wave but also the simulation and calculation of the transmission velocity of the longitudinal and transverse waves through the time travel curve of the vibration velocity of the sound wave at various nodes. Finally, the Hsu-Nielsen lead break experiment was implemented. The results of the theoretical calculation and simulation analysis were consistent with the experimental results, thus demonstrating that the research method using the ANSYS/LS-DYNA software to simulate sound wave transmissions in acoustic emission experiments is feasible and effective.

Keywords: Acoustic emission, Sound velocity, Sound wave, Hsu-Nielsen lead break method, LS-DYNA

1. Introduction

Acoustic emission (AE) is the emission of transient elastic waves resulting from the rapid energy release in a local position in a material. AE technology has been widely used in many fields. AE technology can realize the real-time monitoring of the initiation of structural fatigue cracks and their expansion[1-4].

The identification of the source of structural damage is one of the most important applications of AE techniques. However, the accuracy of AE source identification is low because of inaccuracies in the measured sound velocity and recognition time, background noise, and other factors. Sound wave velocity is an important factor that influences the accurate positioning of AE sources.

Sound velocity, a material property that is closely related to medium density, elasticity modulus, and Poisson's ratio, varies in various media. The transmission velocity in an actual structure is also affected by numerous factors, such as the type of material, anisotropy, and shape and size of the structure. Transmission velocity thus easily varies and is difficult to calculate.

Sound velocity is usually measured experimentally[5-6]. However, experimental measurements show several shortcomings, such as difficulties in changing models, highly restrictive conditions, and potentially high costs. Furthermore, a sound wave is reflected several times during transmission, and each reflection causes pattern changes[7-8]. The effect of wave transmission on a waveform is a basic

problem that must be considered in any experimental setup, data analysis, and evaluation. Therefore, a non-experimental method must be established to measure sound velocity and reveal the transmission characteristics of sound waves.

With the advent of advanced numerical techniques and rapidly enhanced computing power, the direct full-scale simulation of sound wave transmission in AE experiments using the finite element analysis (FEA) method has become increasingly feasible. Wang et al. [9] created a finite element model of AE signal propagation in a slewing ring by using the ANSYS/LS-DYNA software to process the AE signal as a high-frequency stress wave. Zou et al. [10] adopted the ANSYS finite element software to simulate electromagnetic AE. Chen et al. [11] calculated the ultrasonic lamb wave dispersion curve of a thin plate using the finite element method. Roy, A et al. [12] described the simulation of AE waves to identify the source and characteristics of AE in a steel plate, as well as the wave modes. Sause [13] also adopted a new finite element model approach to dynamically change the boundary conditions that simulate crack propagation in a pencil lead. Although FEA software programs have been widely used in correlation analyses for AE, considerably few studies have actually used such software programs to analyze the results of sound velocity simulation.

The present work utilized the ANSYS/LS-DYNA finite element software to analyze the sound waveform generation and propagation in a sheet steel structure. The Hsu-Nielsen lead break experiment was also implemented to evaluate the feasibility of using the finite element software to analyze the AE phenomenon.

* E-mail address: zhangjianchao@yeah.net

2. Key problems in finite element analysis

2.1 Exciting force for lead break

The AE signal at metal breakage is similar to the Hsu-Nielsen lead break signal. Therefore, experimental studies on the characteristic parameters of AE and the localization of the sources of damage often involve the simulation of material breakage and damage with a lead break experiment[14-16].

The AE waveform at a wave source is generally a sharp broadband pulse containing quantitative information about the wave source. Therefore, the exciting force is an important parameter in validating the finite element modeling of a pencil-lead breakage. The time-varying exciting force shown in Equation (1), which generates a waveform similar to that in the Hsu-Nielsen lead break experiment, is employed in this model[17-18] and expressed as

$$F(t) = \begin{cases} 0 & t < 0 \\ 0.5 - 0.5\cos(\pi t / \tau), 0 \leq t \leq \tau \\ 1 & t > \tau \end{cases} \quad (1)$$

2.2 Wave velocity

The characteristics of a material determine the wave velocity. A strong force between neighboring atoms equates to a closely coupled atomic motion. Moreover, a large atomic mass equates to a large amount of force that must be applied under the same level of acceleration. The transmission velocity of an AE wave is a material property closely related to medium density and elasticity modulus. Wave velocity should then be directly proportional to the restoring force between atoms or molecules and inversely proportional to density.

In a homogeneous medium, the theoretical transmission velocities of longitudinal and transverse waves are[19]

$$C_L = \sqrt{\frac{\lambda + 2u}{\rho}} \quad (2)$$

$$C_T = \sqrt{\frac{u}{\rho}} \quad (3)$$

where C_L is the longitudinal wave velocity, C_T is the transverse wave velocity, ρ is the material density, λ is the lame constant, and u is the shear modulus; and

$$\lambda = \frac{\nu E}{(1+\nu)(1-2\nu)} \quad (4)$$

$$u = \frac{E}{2(1+\nu)} \quad (5)$$

where E is the elasticity modulus of the material and ν is the Poisson's ratio of the material.

The following formulas are then derived:

$$C_L = \sqrt{\frac{E}{\rho} \frac{1-\nu}{(1+\nu)(1-2\nu)}} \quad (6)$$

$$C_T = \sqrt{\frac{E}{\rho} \frac{1}{2(1+\nu)}} \quad (7)$$

2.3 Wave length

Sound wave length is an important factor that influences sound wave transmission. The minimum wavelength is

$$\lambda_{\min} = \frac{C}{f_{\max}} \quad (8)$$

where C is the theoretical wave velocity of the testing waveform and f_{\max} is the maximum frequency of the sound wave, which is determined as the frequency of the lead break signal.

3. Establishment of finite element model

3.1 Modeling

The sheet steel used in this experiment measured 508 mm long, 381 mm wide, and 2 mm thick. The texture of the steel was found to be Q235B, and its density, elastic modulus, and Poisson's ratio were 8,240 kg/m³, 2.1 × 10¹¹ Pa, and 0.274, respectively. A coordinate system was also established (Figure 1). The lead break point was set near the left side of the sheet steel, that is, point $X = 500$ mm. Four AE sensors were laid at points a, b, c, and d at an interval of 50 mm.

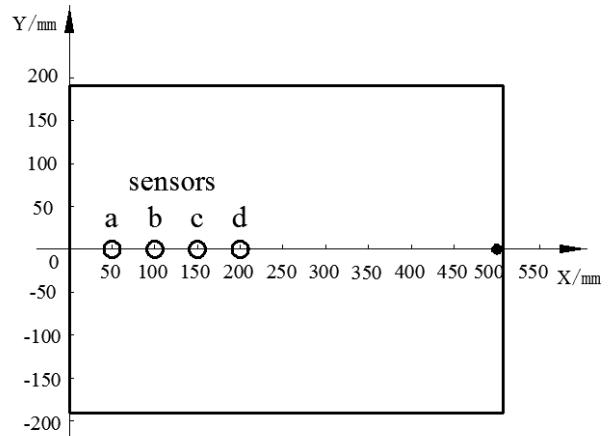


Fig. 1. Sheet steel size and sensor layout

The following steps were employed to establish the finite element model:

(1) Establish the finite element model of sheet steel size and thickness (Fig. 1), with the unit being SHELL163.

(2) Divide the finite element model into a grid size according to the following analysis.

The following parameters were calculated using Equations (1)-(4): frequency of the lead break signal $f_{\max} = 333.3$ kHz, $C_L = 5,815$ m/s, $C_T = 3,208$ m/s, and the transverse and longitudinal wave lengths of 10 and 17 mm, respectively.

The finite element simulation model requires the grid L_e to be at least 1/10 of the wave length λ_{\min} , that is, $L_e \leq \lambda_{\min}/10$. Therefore, $L_e = 1$ mm could meet the requirements[20].

(3) Set up the array of loading time and load value on the basis of Equation (1), as shown in Table 1.

Table 1. Array of loading time and load value

Loading time (μ s)	0	1	2	3	4	5	6	7	8
Load value (N)	0	0.0109	0.0432	0.0955	0.1654	0.2500	0.3455	0.4477	0.5523
Loading time (μ s)	9	10	11	12	13	14	15	1500	
Load value (N)	0.6545	0.7500	0.8346	0.9045	0.9568	0.9891	1	1	

- (4) Generate a component at the node of the lead break position (Figure 1), and apply the aforementioned load array.
- (5) In the output control, set the computation time and computation steps to 150 μ s and 1,000, respectively.

3.2 Visualization results

The simulation results of the AE sound field could be visualized in the “LS-PREPOST” processing module, which

reveals the transmission characteristics of traveling sound waves[21]. Therefore, these transmission characteristics could be applied in the nondestructive testing and simulation of the AE sound field.

Figures 2(a), (b), and (c) show the cloud charts of the Z-directional displacement, speed, and accelerated speed of a sheet steel. The nodes 10927, 19276, 27878, and 36227 are the center of sensors a, b, c, and d (Figure 1), respectively.

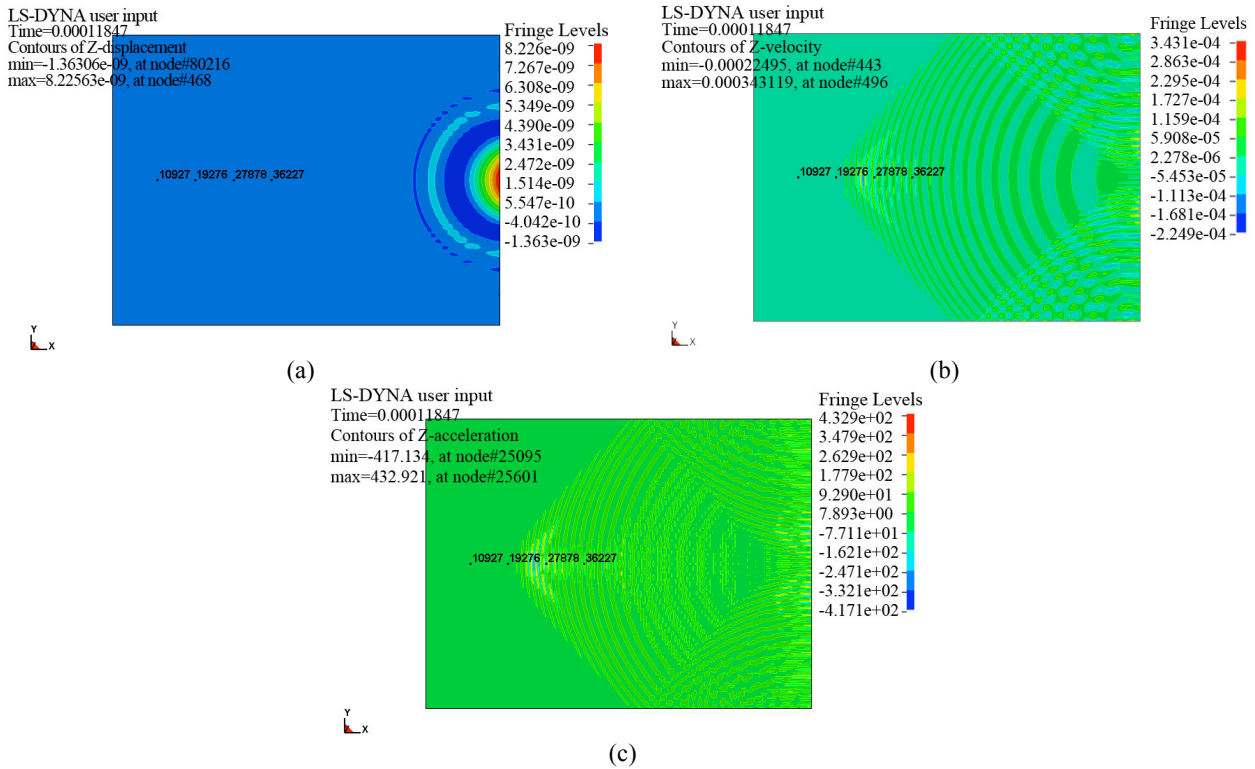


Fig. 2. Cloud chart of Z-directional accelerated speed of the sheet steel

The vibration displacement, speed, and accelerated speed curves of the various nodes along the X, Y, and Z directions during the sound wave transmission could be obtained. Figures 3(a) and (b) show the vibration displacement and

accelerated speed curves, respectively, of node 10927 along the Z direction, and Figure 4(b) shows the speed curve of the node.

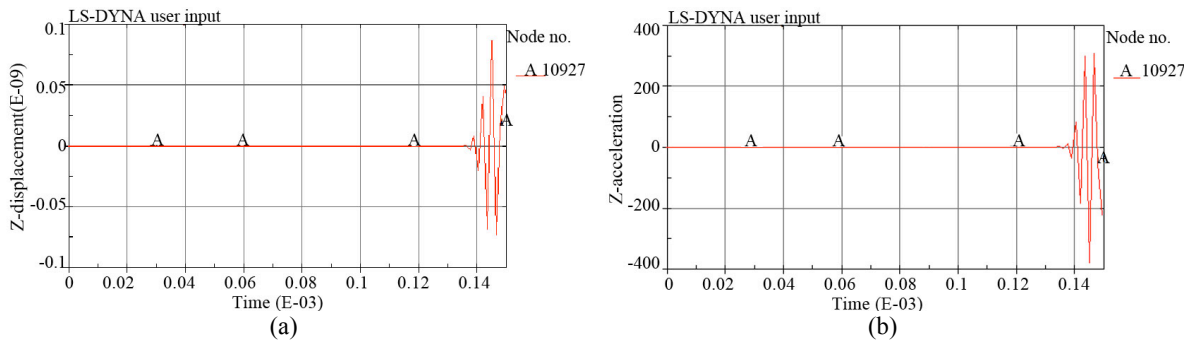


Fig. 3. Vibration of accelerated speed curves of node 10927 along the Z direction

3.3 Simulation calculation of wave velocity

Figures 4(a)-(h) show the vibration velocity time-history curves of nodes 10927, 19276, 27878, and 36227 along the X and Z directions.

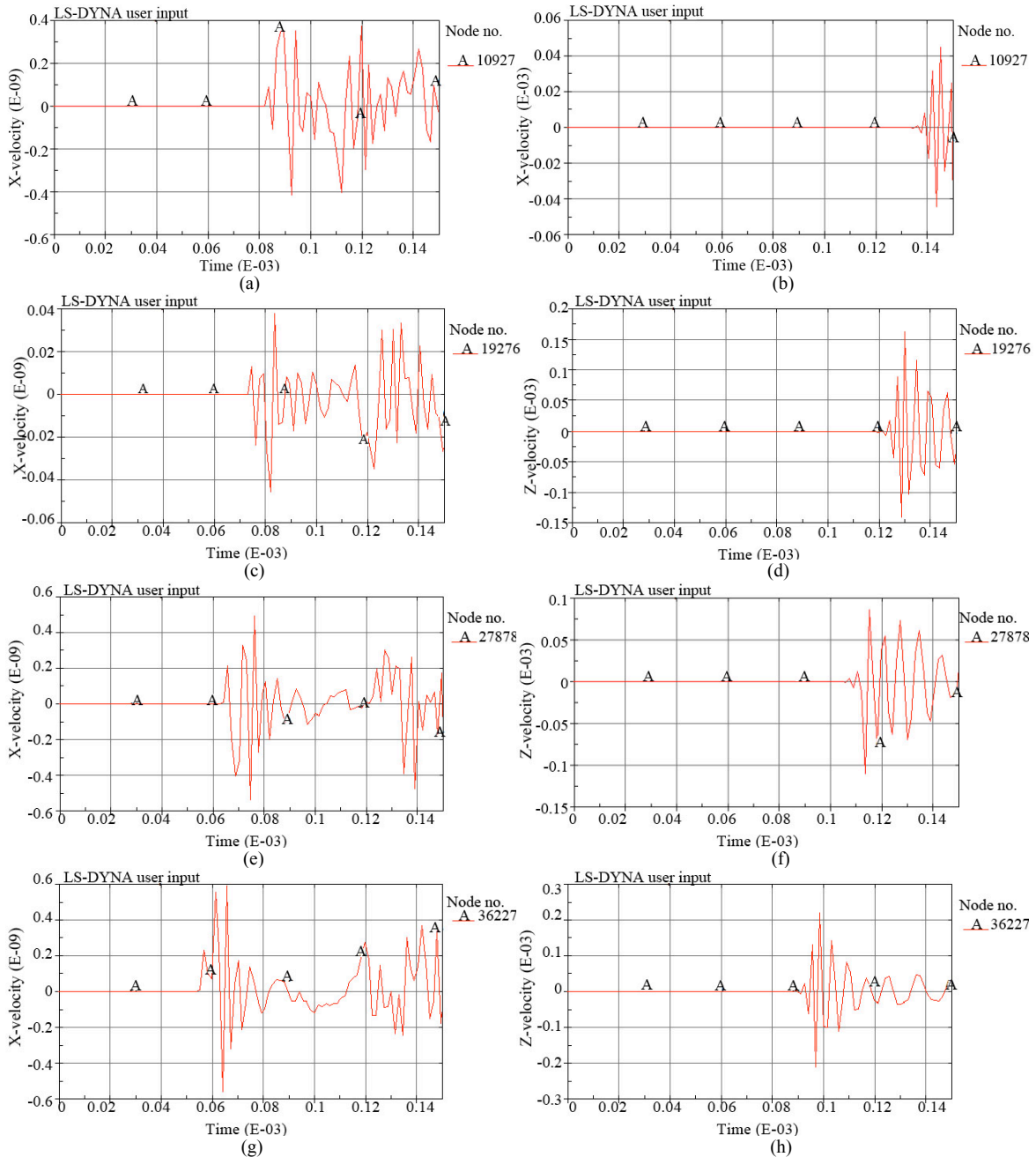


Fig. 4. Vibration velocity time-history curves of node 36227 along the Z direction

Considering the differences in the arrival times of the X-directional and Z-directional vibrations of the four nodes, as well as their amplitude order of magnitude, the X-directional vibration velocity time-history curve of these nodes could be viewed as the transmission of the longitudinal sound wave, whereas the Z-directional vibration could be viewed as the transmission of the transverse sound wave.

On the basis of the X-directional node vibration, we simulated the longitudinal sound wave velocity of the sheet steel. To obtain accurate data on the vibration velocity time-history of the four nodes (Figure 4), we used the numerical values of the MSoft CSV type in the PlotWindow. The velocities and arrival times of the X-directional vibration of nodes 10927, 19276, 27878, and 36227 were recorded, as shown in Table 2 (optional).

The actual sensor has one fixed sensitivity; thus, the vibration amplitude of the nodes was determined to be 9.21×10^{-11} m/s from the vibration amplitude of the nodes along the X direction (Figure 4). The arrive time of the X-directional vibrations of nodes a, b, c, and d at this amplitude was calculated through the interpolation method. The calculated results were then compared with the experimental data.

In the experiment, the interval between the center points of two adjacent sensors was 50 mm. On the basis of the distance between the signal and the two sensors (ΔD), as well as the difference in arrival times (Δt), we deduced that the sound wave velocity is $C = \Delta D / \Delta t$.

The simulation results of the X-directional sound wave velocity could similarly be obtained (data are omitted in this paper).

The simulated sound wave velocities along the X and Z directions are listed in Table 3.

Table 2. X-directional vibration velocities of the four nodes (optional)

Arrival time (s)	X-directional vibration velocities (m/s)				Arrival time (s)	X-directional vibration velocities (m/s)			
	Node a (10927)	Node b (19276)	Node c (27878)	Node d (36227)		Node a (10927)	Node b (19276)	Node c (27878)	Node d (36227)
4.9282E-05	0	0	0	0	6.7451E-05	0	9.3733E-34	-1.9355E-10	-3.1704E-10
5.0775E-05	0	0	0	4.8359E-27	6.8944E-05	0	4.3897E-25	-4.0151E-10	4.5540E-11
5.2268E-05	0	0	0	8.2439E-20	7.0438E-05	0	1.7926E-19	-3.1580E-10	1.7407E-10
5.3762E-05	0	0	0	5.0509E-15	7.1931E-05	0	2.6601E-15	3.3337E-10	-2.0964E-10
5.5255E-05	0	0	0	7.5287E-12	7.3425E-05	0	2.5240E-12	2.4488E-10	-6.4109E-11
5.6997E-05	0	0	0	2.3505E-10	7.4918E-05	0	1.3063E-10	-5.3779E-10	1.3761E-10
5.8491E-05	0	0	1.4794E-34	1.0467E-10	7.6411E-05	1.6959E-31	-2.3612E-10	4.9578E-10	6.1663E-11
5.9984E-05	0	0	1.4619E-24	6.9467E-11	7.7905E-05	1.3947E-24	7.5890E-11	-2.6819E-10	-4.1997E-11
6.1477E-05	0	0	1.0495E-18	5.5755E-10	7.9398E-05	2.1280E-19	9.7575E-11	5.8848E-11	-1.1782E-10
6.2971E-05	0	0	1.5946E-14	2.4211E-10	8.0891E-05	1.9679E-15	-2.5840E-10	1.2624E-10	-9.5319E-11
6.4464E-05	0	0	1.0879E-11	-5.5747E-10	8.2385E-05	1.5706E-12	-4.5605E-10	-1.9714E-10	2.6341E-13
6.5958E-05	0	0	2.1604E-10	5.9725E-10	8.3878E-05	9.2110E-11	3.8153E-10	1.9160E-11	4.2178E-11

Table 3. Simulated sound wave velocities along the X and Z directions

Sensor point	Node number	X position (mm)	X-directional		Z-directional	
			Arrival time (s)	Average velocity (m/s)	Arrival time (s)	Average velocity (m/s)
a	10927	50	8.39×10^{-5}		1.37×10^{-4}	
b	19276	150	7.44×10^{-5}		1.21×10^{-4}	
c	27878	200	6.51×10^{-5}	5,336	1.07×10^{-4}	3,174
d	36227	250	5.59×10^{-5}		8.97×10^{-5}	

4. Experimental study

4.1 Building the experimental system

We built an experimental system to verify the feasibility of the sound wave transmission simulation (Figure 5).

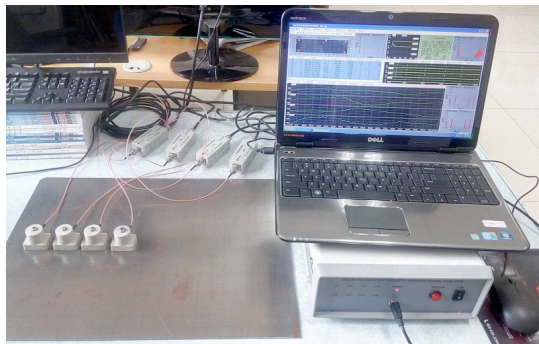


Fig. 5. AE experimental system

The real-time monitoring of AE involved the use of the DS2 series perfect information AE signal analysis system made by Beijing Soft Island Era Technology Co., Ltd. The settings are as follows: the threshold was 20 dB, the pre-amplifier gain was 40 dB; and PDT, HDT, and HLT were 500, 2,000, and 2,000 μ s, respectively.

The sensor model was the SR150M model. The diameter, center frequency, frequency bandwidth, and

interval of the sensors were 19 mm, 0.15 MHz, 60-400 kHz, and 50 mm, respectively.

On the basis of the Nielsen-Hsu lead break method, the HB cartridge (diameter: 0.5 mm) was broken on a plate surface similar to that of the simulated AE source. The lead break experiment was repeated five times at the origin of the coordinate system. The lead break length in each experiment was 2.5 mm, and the lead break direction formed a 30° angle relative to the tested surface.

4.2 Collecting data

In the experiment, the signal received by the AE sensor is not a single-mode wave but rather a superposition of longitudinal, transverse, surface, and plate waves. This superposition becomes increasingly complicated because of the effect of sensor frequency response characteristics. The signal waveform detected in the experiment differed significantly from the original waveform.

The longitudinal mode is the quickest among the four patterns, and it could reduce the effect of wave reflection during measurement and improve the accuracy of the measurement. Therefore, this experiment used the longitudinal sensor to analyze the speed of longitudinal sound wave transmission in verifying the feasibility of the finite element model in wave velocity analysis.

Figure 6 shows the collected signal data in the lead break experiment.

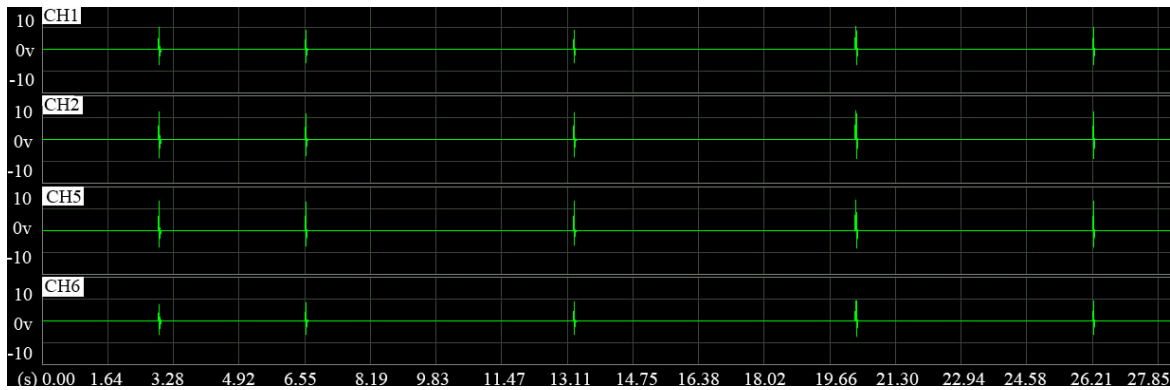


Fig. 6. Signal data collected in the lead break experiment

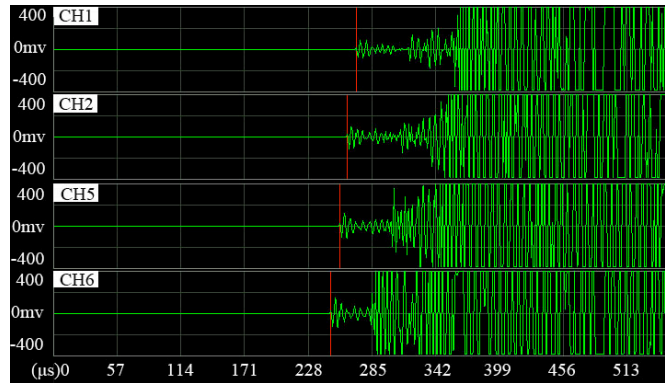


Fig. 7. Trigger position of the third lead break signal

Data on the third pencil-lead break experiment were chosen and amplified locally to obtain the signal trigger position (Figure 7). Table 4 shows the details of the signal trigger time and the experimental results on the longitudinal wave velocity (the time in Figure 7 is the relative time, and the trigger time in Table 4 follows the μs value).

Table 4. Experimental results on the longitudinal wave

Sensor point	X position (mm)	Trigger time (μs)	Average velocity (m/s)
a	50	699	5000
b	150	709	
c	200	717	
d	250	727	

Table 3 and Table 4 show that the simulated wave velocity on the X direction was 5,336 m/s, which indicated a 7.7% deviation from the theoretical longitudinal wave velocity. The simulated wave velocity on the Z direction was 3,174 m/s, with a 1% deviation from the theoretical transverse wave velocity. In the lead break experiment, the longitudinal wave velocity was 5,000 m/s, which equated to a 3.5% deviation from the theoretical value.

The theoretical value, simulation value, and experimental value of the sound wave velocity were consistent, which emphasized the effectiveness of the proposed relative calculation, simulation, and experimental setup.

The causes of the deviations are as follows:

(1) The theoretical wave velocity in an ideal state is the sound wave velocity produced in the lead break experiment. However, wave velocity in an actual structure is influenced by various factors, such as structural shape and size, material type, and content medium, and thus varies. The theoretical

value is unclear and non-authoritative and is only used as a reference value.

(2) Deviations in simulation models are caused by the inaccurate definition of material properties, inadequate precision in geometric modeling, and ambiguous definition of boundary conditions.

(3) Influenced by the frequency response characteristics of sensors and transmission attenuation, signal waveform rise decelerates. This condition occurs along with low amplitude, long duration, delayed arrival, and frequency content skewing to low-frequency ones. Such changes complicate the quantitative analysis of AE waveform and the conventional parameter analysis of waveform.

5. Conclusion

The ANSYS/LS-DYNA FEA software could simulate AE generation and propagation in a structure in a realistic and visual manner. We introduced a method to simulate sound wave velocity. The experimental results are consistent with those of the proposed theoretical calculation and simulation based on the Hsu-Nielsen lead break experiment. This agreement proved the feasibility of the proposed simulation method. The LS-DYNA FEA software is useful in experiments that could not measure wave velocity because it could simulate and calculate wave velocity under experimental conditions at a relatively low cost.

Acknowledgements

The authors are grateful for the support provided by the National Natural Science Foundation of China (No. 11472180) and the Research Fund of Shijiazhuang Tiedao University (No. 20142033).

References

1. K M Holford, R Pullin, S L Evans, M J Eaton, J Hensman, K Worden, "Acoustic emission for monitoring aircraft structures". *Proceedings of the Institution of Mechanical Engineers, Part G: Journal of Aerospace Engineering*, 223(5), 2009, pp.525-532.
2. Jürgen Hesser, Diethelm Kaiser, Heinz Schmitz, Thomas Spies, "Measurements of acoustic emission and deformation in a repository of nuclear waste in salt rock". *Engineering Geology for Society and Territory*, 6, 2014, pp.551-554.
3. Xuesong Han, Tianyu Wu, "Analysis of acoustic emission in precision and high-efficiency grinding technology". *The International Journal of Advanced Manufacturing Technology*, 67(9), 2013, pp.1997-2006.
4. Ryan Jin-Young Kim, Nak-Sam Choi, Jack Ferracane, In-Bog Lee, "Acoustic emission analysis of the effect of simulated pulpal pressure and cavity type on the tooth-composite interfacial de-bonding Ryan". *Dental Materials*, 30(8), 2014, pp.876-883.
5. Felipe Mejia, Mei-Ling Shyu, Antonio Nanni, "Data quality enhancement and knowledge discovery from relevant signals in acoustic emission". *Mechanical Systems and Signal Processing*, 62-63, 2015, pp.381-394.
6. A. Mostafapour, S. Davoodi, M. Gharehaghaji, "Acoustic emission source location in plates using wavelet analysis and cross time frequency spectrum". *Ultrasonics*, 54(8), 2014, pp.2055-2062.
7. Kim Ho Ip, Yiu Wing Mai, "Delamination detection in smart composite beams using lamb waves". *Smart Materials and Structures*, 13(3), 2004, pp.544-551.
8. Ramadas C, Padiyar M J, Balasubramaniam K, Joshi M, Krishnamurthy C V, "Delamination size detection using time of flight of anti-symmetric (A_0) and mode converted A_0 mode of guided Lamb waves". *Journal of Intelligent Material Systems and Structures*, 21(8), 2010, pp.817-825.
9. Xinhua Wang, Jun Liang, Kai Qi, Guanghai Li, "Numerical simulation study on propagation law of acoustic emission signal of slewing ring". *Advances in Acoustic Emission Technology*, Springer New York, 2015, pp.651-666.
10. Qingyang Zou, Xiucheng, Dong, "Finite element simulation of crack testing system of electromagnetic acoustic emission based on ANSYS". *Advanced Materials Research*, 424-425, 2012, pp.1097-1101.
11. Chen Liang, Wang Enbao, Ma Hao, Dong Yanlei, Wang Yu, "Calculation of ultrasonic lamb wave dispersion curve of the thin plate by the finite element method". *Research and Exploration in Laboratory*, 33(11), 2014, pp.28-31.
12. Roy, A, Tan, A.C.C, Gu, Y.T, "Simulation of in plane and out of plane AE source in thin plate". *EDDBE2011 Proceedings*, 2011, pp.318-321.
13. Markus G.R.Sause, "Investigation of pencil-lead breaks as acoustic emission sources". *Journal of Acoustic Emission*, 29, 2011, pp.184-196.
14. Yukiya Yamada, Shuichi Wakayama, Junji Ikeda, Fumiaki Miyaji, "Fracture analysis of ceramic femoral head in hip arthroplasty based on microdamage monitoring using acoustic emission". *Journal of Materials Science*, 46(18), 2011, pp.6131-6139.
15. Yu Jiang, Feiyun Xu, Bingsheng Xu, "Acoustic Emission tomography based on simultaneous algebraic reconstruction technique to visualize the damage source location in Q235B steel plate". *Mechanical Systems and Signal Processing*, 64-65, 2015, pp.452-464.
16. Tian He, Qiang Pan, Yaoguang Liu, Xiandong Liu, Dayong Hu, "Near-field beamforming analysis for acoustic emission source localization". *Ultrasonics*, 52(5), 2012, pp.587-592.
17. Hamstad M.A., "Acoustic emission signals generated by monopole (pencil-lead break) versus dipole sources: finite element modeling and experiments". *Journal of Acoustic Emission*, 25, 2007, pp.92-106.
18. Kwang-Ro Kim, Young-Shin Lee, "Acoustic emission source localization in plate-like structures using least-squares support vector machines with delta t feature". *Journal of Mechanical Science and Technology*, 28(8), 2014, pp.3013-3020.
19. Xu Chao, Shi Zhenming, Gao Yanbin, Zhao Chunfeng, "In situ test in geotechnical engineering". Tongji University Press, Shanghai, 2005.
20. Friedrich Moser, Laurence J. Jacobs, Jianmin Qu, "Application of finite element methods to study transient wave propagation in elastic wave guides". *Review of Progress in Quantitative Nondestructive Evaluation*, 17A, 1998, pp.161-167.
21. Halquist, J. O. "LS-DYNA keyword user's manual version 971". Livermore Software Technology Corporation, Livermore, 2007.